

# Effect of Metal Element in Catalytic Growth of Carbon Nanotubes

Oleg V. Yazyev\* and Alfredo Pasquarello

*Ecole Polytechnique Fédérale de Lausanne (EPFL),*

*Institute of Theoretical Physics, CH-1015 Lausanne, Switzerland and*

*Institut Romand de Recherche Numérique en Physique des Matériaux (IRRMA), CH-1015 Lausanne, Switzerland*

(Dated: November 8, 2018)

Using first principles calculations, we model the chemical vapor deposition (CVD) growth of carbon nanotubes (CNT) on nanoparticles of late transition (Ni, Pd, Pt) and coinage (Cu, Ag, Au) metals. The process is analyzed in terms of the binding of mono- and diatomic carbon species, their diffusion pathways, and the stability of the growing CNT. We find that the diffusion pathways can be controlled by the choice of the catalyst and the carbon precursor. Binding of the CNT through armchair edges is more favorable than through zigzag ones, but the relative stability varies significantly among the metals. Coinage metals, in particular Cu, are found to favor CVD growth of CNTs at low temperatures and with narrow chirality distributions.

PACS numbers: 68.43.Jk, 81.07.De, 81.15.Gh, 82.33.Ya

Carbon nanotubes (CNTs) are expected to become an important constituent of many technologies, in particular of future generation electronics [1]. The inability of performing growth of CNTs with predetermined chirality indices, and thus electronic properties, is the major obstacle on the way to incorporating CNTs into electronic devices. The chemical vapor deposition (CVD) growth of CNTs catalyzed by metallic nanoparticles is believed to be the most promising approach for reaching this goal. This method has already been demonstrated to allow for CNT growth at low temperatures [2] and to yield limited distributions of nanotube chiralities [3, 4].

For a long time, the catalyst composition has been limited to iron-group metals (Fe, Co, Ni) and their alloys. Recently, it has been shown that metallic nanoparticles of many other metals, heavy late transition (Pd, Pt) and inert coinage metals (Cu, Ag, Au), are also able to act as catalysts in the CVD growth process [5, 6]. However, these metals show different physical and chemical properties [7] as a result of the variation of lattice constants,  $d$ -band energies and occupations [8], and relativistic effects [9]. Therefore, important questions arise. What role does the chemical composition of the metal catalyst play in the CVD growth process? To what extent can the choice of the metal catalyst be optimized for achieving deterministic growth of CNTs?

The decomposition of gas-phase carbon precursors on the nanoparticle surface is the first step of the CVD growth of CNTs and can easily be controlled via the thermochemistry. This initial step is followed by two important processes: (i) the diffusion of carbon on the nanoparticle surface or across its interior, and (ii) the nucleation of a graphitic fragment followed by the further incorporation of carbon into the growing nanotube. The diffusion process (i) has been shown to be a rate-limiting step [10, 11], while the chirality of the growing CNT is decided upon the nucleation process (ii) [12, 13]. The catalyst can be either crystalline or liquid [11] during

the growth process but only solid metallic nanoparticles of definite shape can act as templates for the growth of CNTs with specific chiralities [14]. Sufficiently low temperatures are thus necessary for maintaining the crystalline state of nanoparticles during the nucleation stage. Certain technological applications of CNTs also impose restrictions on the processing temperatures [2].

In this work, we investigate the role of the chemical composition of the catalytic nanoparticles in the CVD growth of CNTs using a total-energy scheme. In our study, we consider late transition (Ni, Pd, Pt) and coinage (Cu, Ag, Au) metals. The CVD growth process is analyzed by modeling the diffusion and nucleation steps. For each considered metal, the binding energies of carbon atoms and dimers on the facets as well as in the interior of the nanoparticles are compared. For these carbon species, we then calculate activation energies considering both surface and bulk diffusion pathways. From the stability of zigzag and armchair edges of the growing CNT, we infer the preference for definite chiralities. Our results show that coinage metals, in particular Cu, offer attractive opportunities for growing CNTs at low temperatures and with narrow chirality distributions.

The surface and the interior of metallic nanoparticles were modeled by means of periodic two-dimensional slab and three-dimensional bulk models, respectively. Infinite surfaces were shown to be good models for facets, even in the case of the smallest metallic nanoparticles [17]. We primarily considered the lowest energy (111) facets [20], which dominate the surfaces of fcc-metal nanoparticles [21]. The surfaces were modeled by three-layer slabs with  $p(3\times 3)$  unit cells, which guarantee convergence of relative binding energies within 0.1 eV. We also considered (100) microfaceted surface step-edges, which we modeled by a (311) stepped surface of the same thickness. This model is also a good approximation for extended (100) nanoparticle facets, corresponding to the second largest fraction of the surface area of fcc-metal Wulff clusters.

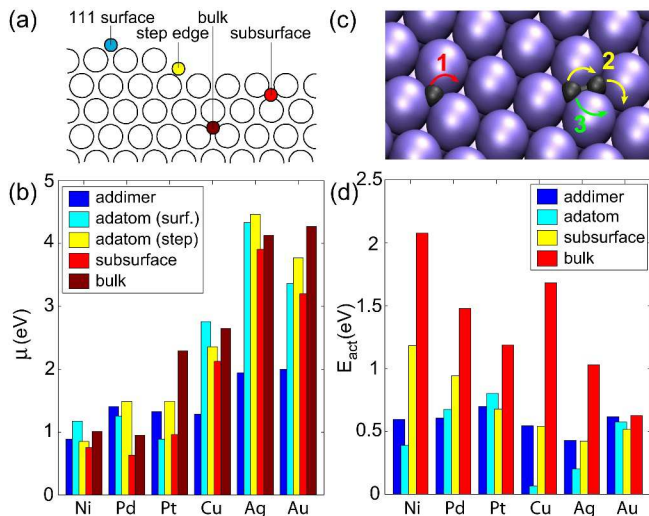


FIG. 1: (Color online) (a) Schematic representation of studied carbon positions at metal surfaces. (b) Chemical potentials of monoatomic and diatomic carbon in different positions expressed with respect to the chemical potential of carbon in graphene. (c) Surface diffusion mechanisms for the carbon adatom (**1**) and the carbon dimer (**2** – concerted mode; **3** – atom-by-atom mode) on a (111) fcc metal surface and (d) respective diffusion barriers for different metals.

In the two-dimensional models, the periodically repeated slabs were separated by at least  $10 \text{ \AA}$  to avoid spurious interactions. The bulk metals were modeled with  $3 \times 3 \times 3$  supercells.

The total energy calculations were performed within a selfconsistent density functional theory framework, as implemented in the PWSCF plane-wave pseudopotential code of the Quantum-ESPRESSO distribution [22]. The Perdew-Burke-Ernzerhof exchange-correlation density functional [23] was used. The ultrasoft pseudopotentials [24] employed in the present study treat the  $d$ -electrons of both transition and coinage metals as valence electrons. The one-electron valence wave functions and the electron density were described by plane-wave basis sets with kinetic energy cutoffs of 25 Ry and 300 Ry, respectively [25]. The Fermi-Dirac function ( $k_B T = 0.01 \text{ Ry}$ ) was used for the population of the one-electron states in metallic systems. For the slab models, a  $4 \times 4 \times 1$   $\mathbf{k}$  point sampling was performed. The bulk supercells were sampled with  $4 \times 4 \times 4$   $\mathbf{k}$  point meshes. The atomic positions of the bottom layer were kept fixed in ideal bulk positions during the relaxation in the slab models. The nudged elastic band method with the climbing-image scheme [26] was used to find the transition states of the diffusion paths.

*Binding of monoatomic and diatomic carbon.* The chemical potential of different forms of carbon expressed with respect to the total-energy per atom of graphene  $\mu_G$  is defined as

$$\mu = \frac{E - E_M}{n_C} - \mu_G, \quad (1)$$

where  $E$  and  $E_M$  are the total energies of the systems with and without carbon, respectively, and  $n_C$  corresponds to the number of carbon atoms. For reference, the chemical potential of the free carbon atom in the spin-triplet ground state is 7.7 eV.

We considered the binding and the diffusion of both carbon atoms and dimers, which are initially produced upon the dehydrogenation of common carbon sources like  $\text{CH}_4$ ,  $\text{C}_2\text{H}_4$ ,  $\text{C}_2\text{H}_2$ , and  $\text{C}_2\text{H}_5\text{OH}$ . For all considered positions [Fig. 1(a)] and metals, the chemical potentials of monoatomic and diatomic carbon are positive, i.e. indicating lower stability than for graphene, and are generally higher for the inert coinage metals [Fig. 1(b)]. On coinage metals, the surface dimers are considerably more stable than all forms of monoatomic carbon. This implies that the diffusion process only involves surface dimers, when the carbon source corresponds to a diatomic carbon precursor such as  $\text{C}_2\text{H}_2$ . At variance, atomic carbon has the lowest chemical potential for late transition metals, as a subsurface interstitial in Ni and Pd and as a surface adatom at the Pt surface.

Adatoms on a (111) surface are threefold coordinated and occupy two different positions, ccp and hcp [17], with chemical potentials differing by less than 0.1 eV. Only the lowest adatom chemical potentials are shown in Fig. 1(b). The highest adatom chemical potential was obtained for Ag, in agreement with the calculations of Abild-Pedersen *et al.* [27] This low stability results from the energy position of the  $d$ -band, which is lowest for this metal [8]. At surface steps, the carbon adatom assumes a semi-octahedral five-fold coordination showing the same local neighborhood as at an adsorption site on the (100) surface. For Ni and Cu the adsorption site at the step is preferred over that on a (111) terrace, as found for Ni in a previous study [18]. However, the converse is true for all heavier metals showing larger lattice constants.

Carbon atoms in subsurface and bulk positions occupy either tetrahedral or octahedral voids, in which they show coordination numbers of 4 and 6, respectively. Subsurface carbon atoms located in voids closest to the surface are more stable than surface carbon adatoms for all metals except Pt. The preferred occupation sites are the tetrahedral voids in Au and Pt characterized by large lattice constants, and octahedral voids in the lighter metals. Only the lowest-energy values are given in Fig. 1(b). Bulk interstitials, i.e. carbon atoms located deep inside the crystalline nanoparticle, have considerably higher chemical potentials than subsurface interstitials due to an enhancement of the elastic response energy [19, 28]. Bulk interstitials preferentially reside in octahedral voids for all metals studied. Subsurface and bulk dimers are found to be highly unstable and are not further discussed here.

*Activation barriers of diffusion.* The relevant diffusion channels of monoatomic and diatomic carbon [Fig. 1(c)] on metallic nanoparticles are addressed through the calculation of their activation barriers  $E_{\text{act}}$  [Fig. 1(d)]. For

monoatomic carbon, we considered surface, subsurface and bulk diffusion modes. In case of diatomic carbon, only the surface diffusion mode was investigated. The reported barrier is the total-energy difference between the transition state and the lowest of the connected minima.

The adatom diffusion barrier is lower for the coinage metals with respect to the late-transition metal belonging to the same row. Moving down the periodic table results in higher diffusion barriers. For the adatom diffusion on the Ni(111) surface, we found a barrier of 0.39 eV, in agreement with previous theoretical estimates [10, 15, 17, 19]. This value is also in fair agreement with the activation energy of the experimental CNT growth process, suggesting that surface diffusion is the rate-limiting step [10, 11]. The adatom diffusion on Cu and Ag surfaces is characterized by surprisingly low barriers of 0.07 eV and 0.20 eV, respectively. This implies that a significant acceleration of the diffusion step can be achieved for these metals when a monoatomic carbon precursor (e.g. CH<sub>4</sub>) is used.

Subsurface and bulk diffusion occur via hopping of interstitial carbon atoms between adjacent tetrahedral and octahedral voids. The diffusion barriers for this channel is generally higher than for adatom diffusion. However, the activation energy for subsurface diffusion decreases with increasing lattice constant, following an opposite trend with respect to the adatom diffusion and leading to competition between the two diffusion modes for the heaviest metals. Activation barriers of subsurface diffusion are always lower than those of the corresponding bulk diffusion due to the reduced elastic response in proximity of the nanoparticle surface. However, in the particular case of Au, activation energies for surface, subsurface, and bulk diffusion fall in a narrow range between 0.52 and 0.64 eV, implying that monoatomic carbon in gold can diffuse uniformly across the nanoparticle already at low temperatures.

When the carbon precursor gives rise to diatomic carbon, the dimer diffusion channel becomes relevant. We considered two different mechanisms for the surface dimer diffusion, the concerted and the atom-by-atom modes, as illustrated pictorially in Fig. 1(c). For the metals studied, the concerted mode shows activation barriers exhibiting small variations. Calculated values range between 0.43 eV for Ag and 0.70 eV for Pt, and are comparable to the diffusion barrier of the carbon adatom on Ni(111). The atom-by-atom mode yields higher diffusion barriers with energy differences ranging from almost zero for Pt to 0.62 eV for Ni. In Fig. 1(d), the activation energies reported for dimer diffusion correspond to the lowest energy mode, i.e. to the concerted mode.

*Binding of CNT to metal nanoparticle.* To understand the relation between the chirality of the growing CNT and the chemical composition of the catalyst, a comprehensive study of the interaction between graphitic fragments and metallic nanoparticles is required. However,

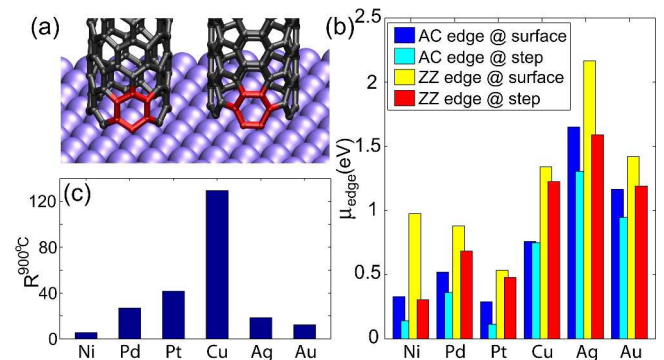


FIG. 2: (Color online) (a) Schematic representation of the binding of ZZ (left) and AC (right) carbon nanotube to a flat (111) surface of the catalyst nanoparticle. The edge fragments used to model the interaction between the nanotube and the nanoparticle surface are shown in red. (b) Chemical potentials of edge atoms of AC and ZZ fragments bound to the metal surfaces and steps. The chemical potential of carbon atoms at free AC and ZZ edges are 2.13 eV and 2.83 eV, respectively. (c) Thermodynamic chirality preference ratios at a synthesis temperature of 900°C for various metal catalysts.

such an investigation is computationally prohibitive because of the large configuration space involved [12, 13]. To address this issue, we here focused on the binding of minimal structural units of armchair (AC) and zigzag (ZZ) edges to either flat or stepped surfaces. We modeled AC and ZZ edges by 1,2-didehydrobenzene (C<sub>6</sub>H<sub>4</sub>) and dehydrobenzene (C<sub>6</sub>H<sub>5</sub>) molecules having 2 and 1 edge atoms, respectively, as illustrated in Fig. 2(a).

The binding energies are quantified by the chemical potential per edge atom  $\mu_{\text{edge}}$  defined as

$$\mu_{\text{edge}} = \mu_{\text{edge}}^{\text{free}} + \frac{E - E_{\text{frag}} - E_{\text{M}}}{n_{\text{C}}}, \quad (2)$$

where  $\mu_{\text{edge}}^{\text{free}}$  is the chemical potential per edge atom for an unbound edge,  $E_{\text{frag}}$  the total energy of an isolated model fragment, and  $n_{\text{C}}$  the number of edge atoms. We estimated  $\mu_{\text{edge}}^{\text{free}}$  through the calculations of ideal graphene and suitable graphene nanoribbons. For  $\mu_{\text{edge}}^{\text{free}}$  of AC and ZZ edges, we found values of 2.13 eV and 2.83 eV, in good agreement with previously reported results [16].

The calculated chemical potentials  $\mu_{\text{edge}}$  corresponding to optimally placed fragments bound to either facets or step-edges are given in Fig. 2(b) for the various metals. These results show that all studied metals share common qualitative features: (i) The chemical potentials  $\mu_{\text{edge}}$  are always lower than  $\mu_{\text{edge}}^{\text{free}}$ , implying that the binding of the graphitic fragment to the metallic nanoparticles is energetically favored. Binding to step-edges is systematically preferred over binding to flat terraces, in accord with experimental indications [14, 29]. (ii) The chemical potentials  $\mu_{\text{edge}}$  in Fig. 2(b) and those of mono-atomic and di-atomic species in Fig. 1(b) exhibit similar behavior as the metal is varied, consistent with the properties

of the metal  $d$ -band [8]. However, the former chemical potentials are always lower for corresponding metals, indicating that the aggregation of bound C atoms in the form of graphitic fragments is energetically favored. (iii) The chemical potentials  $\mu_{\text{edge}}$  are always positive, i.e. the C atoms are less stable than in the reference ideal graphene, suggesting that there exists a driving force towards extending the size of graphitic aggregates. The combination of these three features points to the existence of a negative chemical potential gradient for the nucleation and further growth of CNTs from a carbon feedstock. This supports the catalytic activity of a wide range of metals, including the inert coinage metals.

The chemical potentials  $\mu_{\text{edge}}$  in Fig. 2(b) also provide insight into the ability of different metal catalysts of growing CNTs with definite chiralities. For all considered metals, AC edges are found to be more stable than ZZ edges. In order to provide a more quantitative measure of this preference at a growth temperature  $T$ , we define the ratio

$$R^T = \exp \left[ -\frac{\mu_{\text{edge}}^{\text{AC}} - \mu_{\text{edge}}^{\text{ZZ}}}{kT} \right], \quad (3)$$

assuming that the CNT nucleation occurs under thermodynamic control. For a graphitic CNT nucleus, the chemical potential of the edge carbon atoms is higher than that of the other carbon atoms, leading to the growth of CNT with minimal edge perimeters. Under this assumption, the ratio  $R^T$  characterizes the distribution of CNT chiralities indicating the preference of growing AC-like or ZZ-like CNTs. Ultimate selectivity is achieved for ZZ and AC CNTs for  $R^T=0$  and  $R^T \rightarrow \infty$ , respectively.

Figure 2(c) shows  $R^T$  for the different metal catalysts at a typical CVD synthesis temperature of 900°C. All metals show a strong preference for growing AC rather than ZZ nanotubes, in agreement with experimental reports for iron-group transition metals [3]. In Fig. 2(c),  $R^{900^\circ\text{C}}$  ranges between 5 for Ni and 130 for Cu. The case of Cu is particularly noteworthy for several reasons. First, its high value of  $R^T$  implies that the CNTs grown on Cu nanoparticles are highly enriched by metallic AC species, in accordance with preliminary experimental reports [6]. Second, Cu features the lowest carbon diffusion barriers suggesting that CVD synthesis could take place at much lower temperatures. In these conditions, the chirality preference ratio  $R^T$  would be further enhanced. Third, for Cu, the chemical potentials in Fig. 2(b) show that graphitic fragments indifferently bind to flat or stepped surfaces, suggesting that step-edge formation on Cu nanoparticles is not likely to occur during the nucleation of carbon nanotubes [14, 29]. Preserving the shape of the nanoparticle is a prerequisite for the realization of chirality-specific CNT growth on predetermined catalytic templates.

In conclusion, our study of the diffusion and nucleation stages of CVD growth of CNTs highlights the potential of

catalytic nanoparticles of coinage metals. For these metals, the stability and the diffusion barriers of diatomic carbon allow one to restrict the diffusion pathways to the nanoparticle surface by choosing an appropriate gas-phase carbon source. Furthermore, particularly low diffusion barriers are found for carbon adatoms in the case of Cu and Ag, suggesting the possibility of realizing growth at low growth temperatures. The Cu catalyst is also found to be the most promising candidate for growing carbon nanotubes of definite chirality.

We acknowledge useful discussions with L. Forró, K. Lee, A. Magrez, and Ž. Šljivančanin. We used computational resources at CSCS.

---

\* oleg.yazyev@epfl.ch

- [1] R. H. Baughman, A. A. Zakhidov, and W. A. de Heer, *Science* **297**, 787 (2002).
- [2] M. Cantoro *et al.*, *Nano Lett.* **6**, 1107 (2006).
- [3] S. M. Bachilo *et al.*, *J. Am. Chem. Soc.* **125**, 11186 (2003).
- [4] Y. Miyauchi *et al.*, *Chem. Phys. Lett.* **387**, 198 (2004).
- [5] D. Takagi *et al.*, *Nano Lett.* **6**, 2642 (2006).
- [6] W. Zhou *et al.*, *Nano Lett.* **6**, 2987 (2006).
- [7] H. Okamoto, *Desk Handbook. Phase Diagrams for Binary Alloys* (ASM International, Materials Park, 2000).
- [8] B. Hammer, Y. Morikawa, and J. K. Nørskov, *Phys. Rev. Lett.* **76**, 2141 (1996).
- [9] H. Häkkinen, M. Moseler, and U. Landman, *Phys. Rev. Lett.* **89**, 033401 (2002).
- [10] S. Hofmann *et al.*, *Phys. Rev. Lett.* **95**, 036101 (2005).
- [11] K. Bartsch *et al.*, *J. Appl. Phys.* **97**, 114301 (2005).
- [12] S. Reich, L. Li, and J. Robertson, *Phys. Rev. B* **72**, 165423 (2005).
- [13] S. Reich, L. Li, and J. Robertson, *Chem. Phys. Lett.* **421**, 469 (2006).
- [14] H. Zhu *et al.*, *Small* **1**, 1180 (2005).
- [15] S. Helveg *et al.*, *Nature* **427**, 426 (2004).
- [16] X. Fan *et al.*, *Phys. Rev. Lett.* **90**, 145501 (2003).
- [17] Q.-M. Zhang *et al.*, *Phys. Rev. B* **69**, 205413 (2004).
- [18] H. S. Bengaard *et al.*, *J. Catal.* **209**, 365 (2002).
- [19] F. Abild-Pedersen *et al.*, *Phys. Rev. B* **73**, 115419 (2006).
- [20] L. Vitos *et al.*, *Surf. Sci.* **411**, 186 (1998).
- [21] F. Baletto and R. Ferrando, *Rev. Mod. Phys.* **77**, 371 (2005).
- [22] S. Baroni *et al.*, <http://www.quantum-espresso.org/>.
- [23] J. P. Perdew, K. Burke, and M. Ernzerhof, *Phys. Rev. Lett.* **77**, 3865 (1996).
- [24] D. Vanderbilt, *Phys. Rev. B* **41**, R7892 (1990).
- [25] A. Pasquarello *et al.*, *Phys. Rev. Lett.* **69**, 1982 (1992); K. Laasonen *et al.*, *Phys. Rev. B* **47**, 10142 (1993).
- [26] G. Mills, H. Jónsson, and G. K. Schenter, *Surf. Sci.* **324**, 305 (1995); G. Henkelman, B. P. Uberuaga, and H. Jónsson, *J. Chem. Phys.* **113**, 9901 (2000).
- [27] F. Abild-Pedersen *et al.*, *Phys. Rev. Lett.* **99**, 016105 (2007).
- [28] M. Todorova *et al.*, *Phys. Rev. Lett.* **89**, 096103 (2002).
- [29] J. A. Rodriguez-Manzo *et al.*, *Nat. Nanotechnol.* **2**, 307 (2007).